



TITLE:

Experimental and Analytical Investigation on the Nonlinear Behaviors of Glulam Moment-Resisting Joints Composed of Inclined Self-Tapping Screws with Steel Side Plates

AUTHOR(S):

Komatsu, Kohei; Teng, Qicheng; Li, Zherui; Zhang, Xiaolan; Que, Zeli

CITATION:

Komatsu, Kohei ...[et al]. Experimental and Analytical Investigation on the Nonlinear Behaviors of Glulam Moment-Resisting Joints Composed of Inclined Self-Tapping Screws with Steel Side Plates. *Advanced in Structural Engineering* 2019, 22(15): 3190-3206

ISSUE DATE:

2019-11-01

URL:

<http://hdl.handle.net/2433/255610>

RIGHT:

This is the accepted manuscript of the following article: Komatsu K, Teng Q, Li Z, Zhang X, Que Z. Experimental and analytical investigation on the nonlinear behaviors of glulam moment-resisting joints composed of inclined self-tapping screws with steel side plates. *Advances in Structural Engineering*. 2019;22(15):3190-3206. doi:10.1177/1369433219858722.; This is not the published version. Please cite only the published version.; この論文は出版社版ではありません。引用の際には出版社版をご確認ください。



Experimental and Analytical Investigation on the Nonlinear Behaviors of Glulam Moment-Resisting Joints Composed of Inclined Self-Tapping Screws with Steel Side Plates

Journal:	<i>Advances in Structural Engineering</i>
Manuscript ID	ASE-18-0857.R1
Manuscript Type:	Original Research
Date Submitted by the Author:	02-May-2019
Complete List of Authors:	Komatsu, Kohei; Nanjing Forestry University, College of Materials Science and Engineering; Kyoto University Teng, Qicheng; Nanjing Forestry University; Baoguoqi Ancient Architecture Museum LI, ZHERUI; Nanjing Forestry University; Kyoto University Zhang, Xiao-Lan; Nanjing Forestry University; Kyoto University Que, Zeli; Nanjing Forestry University, Department of Timber Structures
Keywords:	Glulam, Self-Tapping Screw, Steel Side Plate, Beam-Column Joint, Normalized Characteristic Loop (NCL) Model
Abstract:	Glulam moment-resisting joint composed of inclined self-tapping-screws (STS) with steel side plates were designed and its nonlinear moment-rotational skeleton curve was predicted by taking nonlinear load(P)-deformation(u) relationships of all moment-resisting components into considerations within step-wise linear calculation process. P-u relationships of all moment-resisting components were estimated by the fundamental shear joint tests or appropriate empirical relationships and they were approximated by the tetra polygonal-line curves or bi-linear curves. The extended Normalized Characteristic Loop (NCL) model, which was originally developed for RC construction, was applied to describe the hysteresis loops. For predicting failure load, the design equations for a mechanical joint loaded with inclination to the grain direction were applied. Three replications of T-shaped beam-column joint specimens were fabricated using Canadian spruce glulam beam and column. Connections of steel plates to glulam members were all composed of full-threaded inclined-STs. Static push-pull cyclic loading tests were conducted and observed behaviors were compared with step-wise linear analytical results. Agreements between predicted nonlinear behaviors and observed ones were good on the whole.

SCHOLARONE™
Manuscripts

1
2
3
4
5
6
7
8
9
10
11
12
13
14
15
16
17
18
19
20
21
22
23
24
25
26
27
28
29
30
31
32
33
34
35
36
37
38
39
40
41
42
43
44
45
46
47
48
49
50
51
52
53
54
55
56
57
58
59
60

Experimental and Analytical Investigation on the Nonlinear Behaviors of Glulam Moment-Resisting Joints Composed of Inclined Self-Tapping Screws with Steel Side Plates

Kohei Komatsu^{1,2}, Qicheng Teng^{1,3}, Zherui Li^{1,2}, Xiaolan Zhang^{1,2}, and Zeli Que^{1*a}

1: Department of Timber Structures, College of Material Science and Engineering,
Nanjing Forestry University, Nanjing, China

2: Research Institute for Sustainable Humanosphere, Kyoto University, Uji, Japan

3: Baoguosi Ancient Architecture Museum, Ningbo, China

*a: Corresponding Author

E-mail: zeli.que@njfu.edu.cn

Postal address: No.159 Lonpan Road, Nanjing, 210037, Jiangsu Province, CHINA

Key-words: Glulam, Self-Tapping Screw, Steel Side Plate, Beam-Column Joint, Normalized Characteristic Loop (NCL) Model

Abstracts

Glulam moment-resisting joint composed of inclined self-tapping-screws (STS) with steel side plates were designed and its nonlinear moment-rotational skeleton curve was predicted by taking nonlinear load(P)-deformation(u) relationships of all moment-resisting components into considerations within step-wise linear calculation process. P-u relationships of all moment-resisting components were estimated by the fundamental shear joint tests or appropriate empirical relationships and they were approximated by the tetra polygonal-line curves or bi-linear curves. The extended Normalized Characteristic Loop (NCL) model, which was originally developed for RC construction, was applied to describe the hysteresis loops. For predicting failure load, the design equations for a mechanical joint loaded with inclination to the grain direction were applied. Three replications of T-shaped beam-column joint specimens were fabricated using Canadian spruce glulam beam and column. Connections of steel plates to glulam members were all composed of full-threaded inclined-STs. Static push-pull cyclic loading tests were conducted and observed behaviors were compared with step-wise linear analytical results. Agreements between predicted nonlinear behaviors and observed ones were good on the whole.

1
2
3
4
5
6
7
8
9 **1. Introduction**

10 **1.1 Glulam moment-resisting joint (MRJ)**

11
12 MRJ is now popular for constructing glulam portal frame structures. Although the first effective
13 connecting method for glulam portal frames were nails with steel gusset plates (Buchanan and
14 Fairweather, 1993; Komatsu, 2017), drift-pins with insert steel gusset plates were preferably used
15 in Japan due to its aesthetic outlook and better fire endurance performance (Komatsu,2017;
16 Komatsu, 1991). In addition to these conventional connection methods, glued-in-rod (GIR)
17 connection (Riberholt, 1986) also became popular (Buchanan and Fairweather, 1993). Due to its
18 excellent structural, aesthetic and fire-endurance performances, GIR connection became one of the
19 most popular methods for constructing glulam constructions in the world.
20
21
22
23
24

25 **1.2 Engineered use of self-tapping screw (STS)**

26
27 Use of STS is a new trend in recent research field on timber engineering. There are two different
28 roles for the use of STS. Blaß and Schmid (2001), Blaß and Bejtka (2004, 2005, 2006) proposed a
29 lot of practical methods for reinforcing weak points of timber using STS. Another interesting use of
30 STS is to utilize its higher stiffness and strength performance of “inclined tensile shear joint”. This
31 excellent performance was first reported by Blaß and Bejtka (2002) and Kevarinmäki (2002). After
32 these pioneering researches, extensive researches on timber-to-timber tensile shear joint
33 performances have been published up to today (Pirnbacher et al., 2009; Frese and Blaß,2009;
34 Tomasi et al., 2010; Jockwer et al., 2014; Ringhofer et al., 2015; Girhammar et al., 2017; Brandner
35 et al., 2018). Research, however, on the performance of timber-to-steel inclined STS joint was, so
36 far as we know, only one given by Krenn and Schickhofer (2009).
37
38
39
40
41
42

43 **1.3 Research purpose**

44
45 In our study, we paid our attention to the **excellent performance of timber-to-steel inclined STS**
46 **joint with referring to the previous researches (Blaß and Bejtka, 2002; Kevarinmäki,2002; Krenn**
47 **and Schickhofer, 2009)**. We expected the tensile inclined STS to play a role as the tensile-resisting
48 component for the glulam beam-column MRJ. While for the compressive-resisting component, we
49 expected the contributions from the compressive inclined STS joint and the contact of glulam on
50 the steel base plate. Consequently, the main purpose of this study is to verify the analytical
51 procedures applied to the glulam beam-column MRJ specimens whose joint performances were not
52 only largely different between the tensile side and compressive side of the beam member but also
53
54
55
56
57
58
59
60

1
2
3
4
5
6
7
8
9
10
11
12
13
14
15
16
17
18
19
20
21
22
23
24
25
26
27
28
29
30
31
32
33
34
35
36
37
38
39
40
41
42
43
44
45
46
47
48
49
50
51
52
53
54
55
56
57
58
59
60

1 having large nonlinearities. We used three replications of the glulam beam-column MRJ specimens
2 in this study.

3
4 **1.4 Descriptions of the MRJ developed in this article**

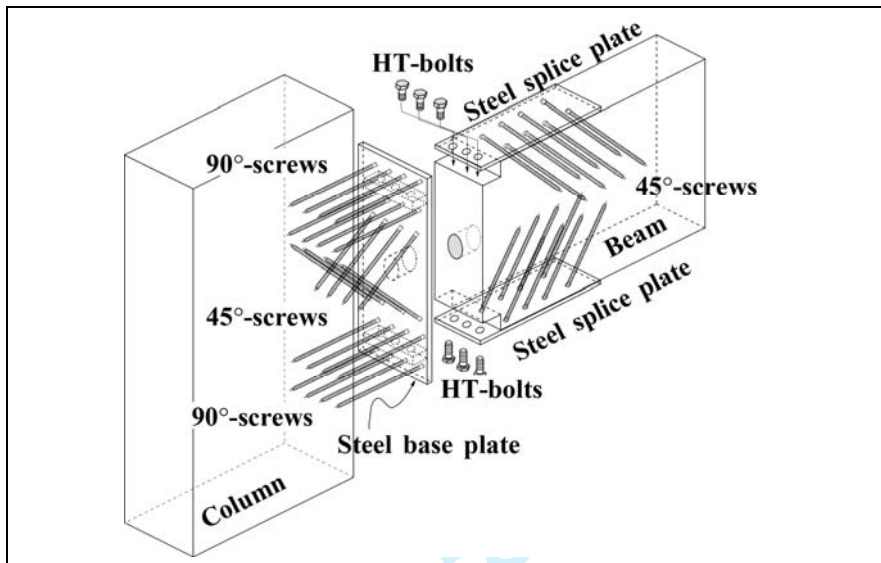


Fig.1 Perspective view of glulam beam-column MRJ designed in this study.

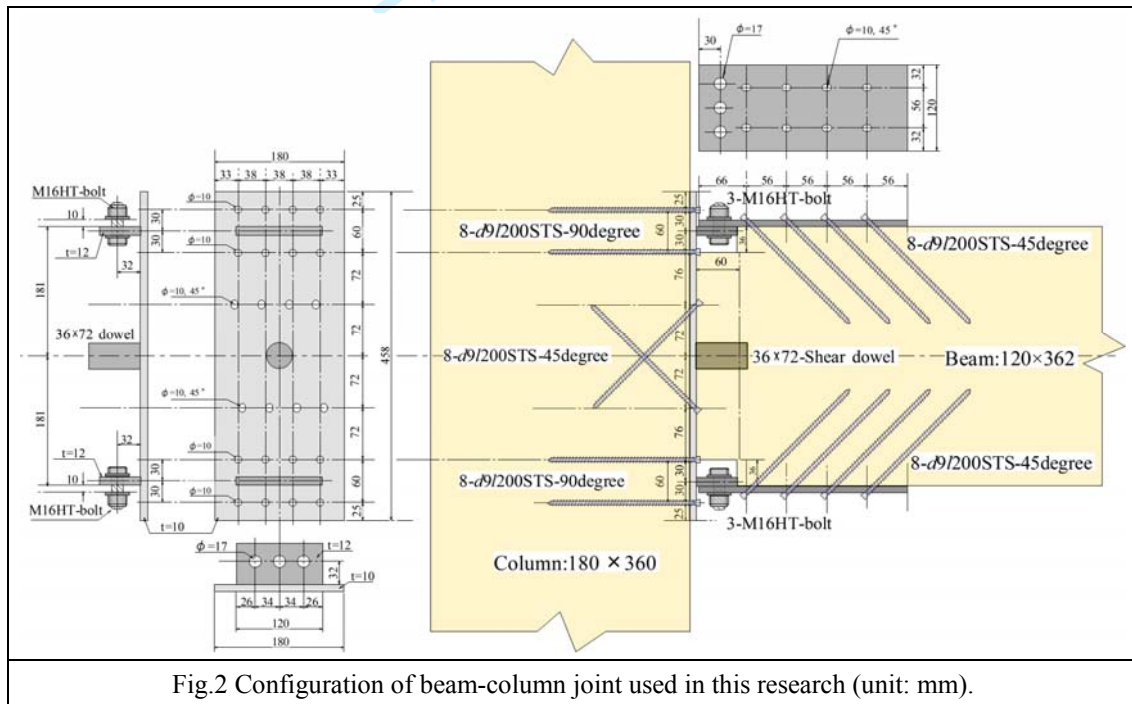
6
7 Figure 1 shows a perspective view of the MRJ beam-column joint designed in this study. For
8 the beam-side joint, referring to the results of Krenn and Schickhofer (2009), 45-degree inclined
9 STS joints with steel side plates were used for resisting against moment. A large cross sectional
10 steel dowel was employed for resisting against the shear force in the beam member.

11 For the column-side joint, ordinary 90-degree STS joints were used for resisting against moment
12 because they can take the maximum pull-out value at 90 degree (EC-5,2008; Hübner et al., 2010).
13 While at the middle of column-side joint, 45-degree inclined X-shape STS were used for resisting
14 against the shear force in the column member. We considered the following moment-resisting
15 components such as the tensile and compressive forces due to the inclined STS joints, contact force
16 of beam end-grain surface to the steel base plate and that of column side-grain surface to the steel
17 base plate.

2. Experiments

2.1 Configuration of beam-column joint

Figure 2 shows the configuration of beam (120 mm × 362 mm) to column (180 mm × 360 mm) joint designed in this study. This configuration was determined mainly considering the size of STS available. For the steel plates composing II-shaped jig, SS400 steel plates of 10 mm thickness were used. For the connecting parts between splice plate and base plate, SS400 steel plates of 12 mm thickness were used and they were welded to each other with the right angle. Over-size of all lead-holes for the STS was 1 mm. Connections between steel plates were done using M16 High Tension (HT)-bolts by introducing torque of 300Nm, in accordance with manufacturer's instruction (NIPPON STEEL BOLTEN CORPORATION, 2019).



2.2 Materials

2.2.1 Glulam

Glulam used in this study was produced in a Chinese glulam company in accordance with Chinese production standard (GB/T 26899-2011, 2011) using imported Canadian spruce (*Picea lauca* (Moench) Voss) lamina. The category of the glulam was the “same-grade composition”

1
2
3
4
5
6
7
8
9
10
11
12
13
14
15
16
17
18
19
20
21
22
23
24
25
26
27
28
29
30
31
32
33
34
35
36
37
38
39
40
41
42
43
44
45
46
47
48
49
50
51
52
53
54
55
56
57
58
59
60

1 structural glulam (GB/T 26899-2011, 2011). Physical and mechanical properties of glulam used are
2 shown in Table 1. All these values were measured by the authors.

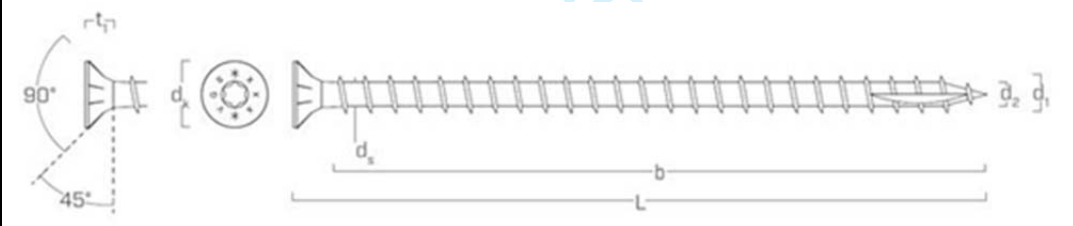
3
4 Table 1 Physical and mechanical properties of glulam used in this research

	Density ρ	Modulus of Elasticity E	Glue-line shear strength f_s
Unit	kg/m ³	N/mm ²	N/mm ²
Number of sample	23	4	23
Mean value	449	11493	6.2
Standard deviation	37.5	927	0.62
Test standard	GB/T 1933-2009	GB/T 50329-2012	

5
6 **2.2.2 Screw**

7 In this study, STS made of carbon steel, which is electrogalvanized with trivalent chromium,
8 having 1000kN/mm² of yielding strength (ROTHO BLAAS SRL, 2019), was used. Figure3 shows
9 the profiles of the STS used in this study.

10



Code name	Nominal diameter	Head diameter	Tip diameter	Shank diameter	Head height	Total length	Thread part length
VGS9200	d ₁ (mm)	d _k (mm)	d ₂ (mm)	d _s (mm)	t ₁ (mm)	L (mm)	b (mm)
	9	16	5.9	6.5	6.5	200	190

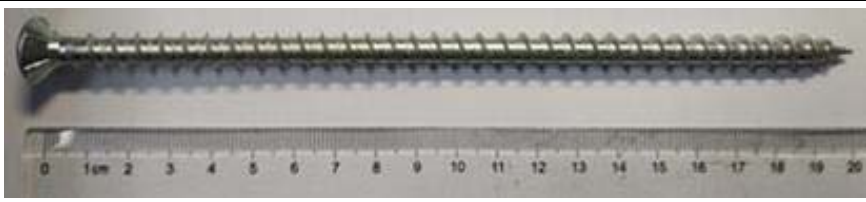
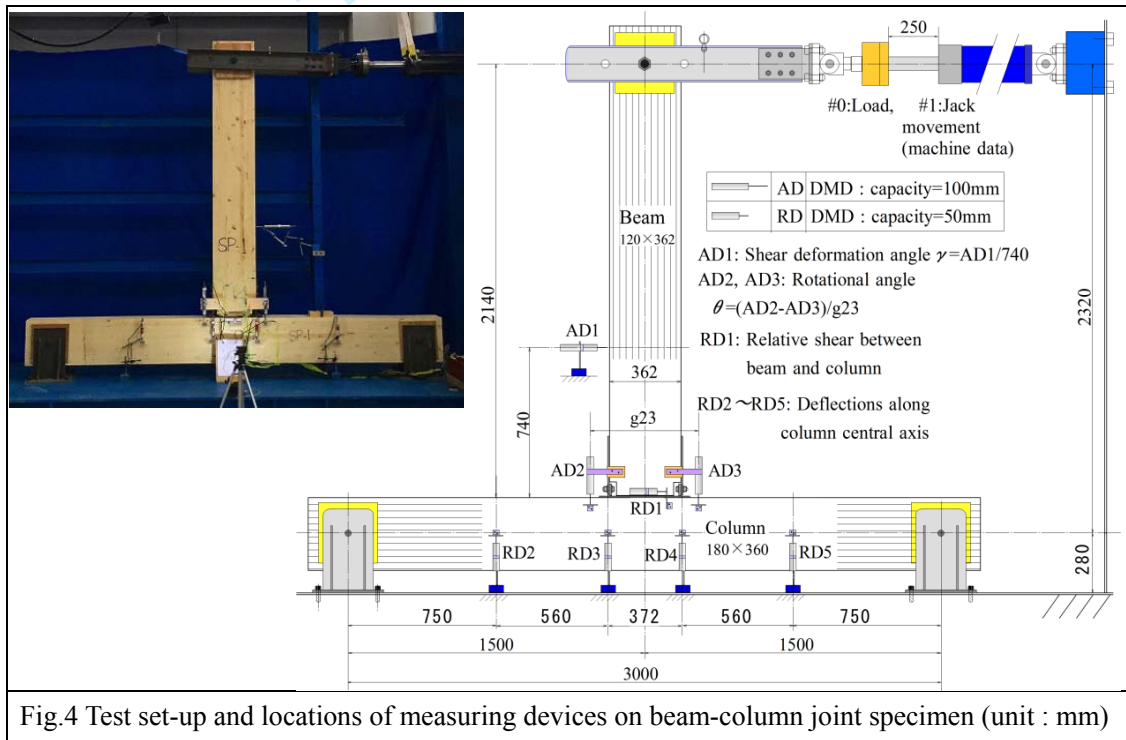


Fig.3 Full-threaded STS used in this study (ROTHO BLAAS SRL, 2019)

2.3 Beam-Column Joint Test

2.3.1 Test set-up

Figure 4 shows the test set-up of the beam-column joint specimen and locations of deflection measuring device (AD1 to AD3 and RD1 to RD5). The aims of each deflection measuring devices were explained in the Fig.4. Horizontal load was applied by an oil-jack having a maximum capacity of 250kN and a maximum stroke of 500mm. Movement of oil-jack was controlled automatically in accordance with an assigned loading protocol shown in 2.3.2, which was preliminarily inputted into the computer of the testing machine (YAW-250J).



2.3.2 Loading protocol

Pull-push cyclic load was applied statically in 11 incremental deformation steps with three repeated cycles in the same peak shear deformation angle ($\gamma = \delta/H$) where δ was loading point displacement, H was distance between loading point and rotation point (2140 mm).

Figure 5 shows the loading protocol expressing by the loading point displacement (δ). At the last 12th step, after pull-load was applied until P_{max} , loading was continued until it dropped lower

1
2
3
4
5
6
7
8
9
10
11
12
13
14
15
16
17
18
19
20
21
22
23
24
25
26
27
28
29
30
31
32
33
34
35
36
37
38
39
40
41
42
43
44
45
46
47
48
49
50
51
52
53
54
55
56
57
58
59
60

1 than 80 % of P_{max} , afterwards oil-jack was returned back to the neutral position. This loading
2 protocol was referred to that assigned by Japan Housing and Wood Technology Center (2008).
3

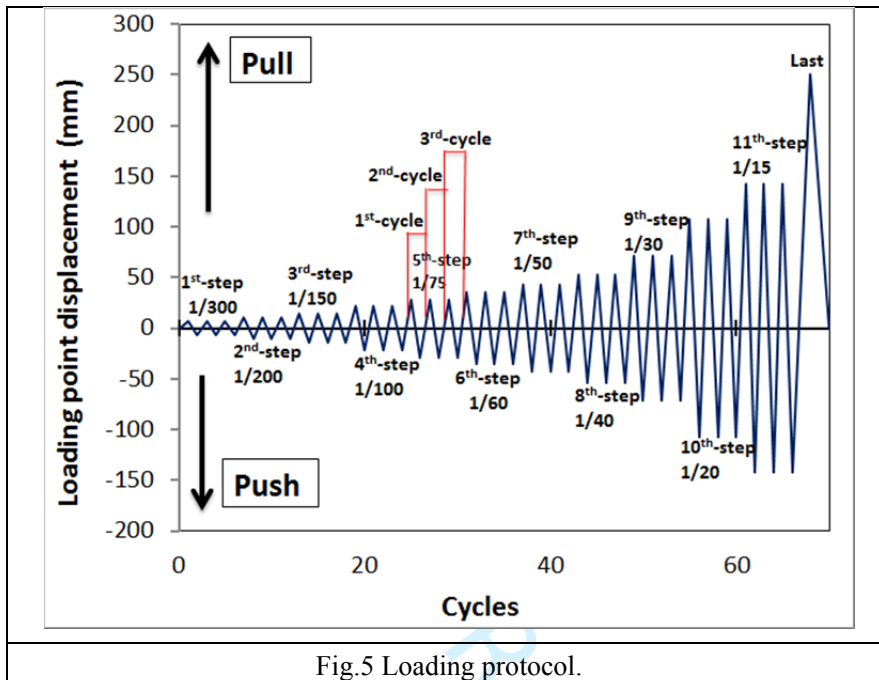


Fig.5 Loading protocol.

4
5
6
7
8
9

2.4 Fundamental Joint Test on STS

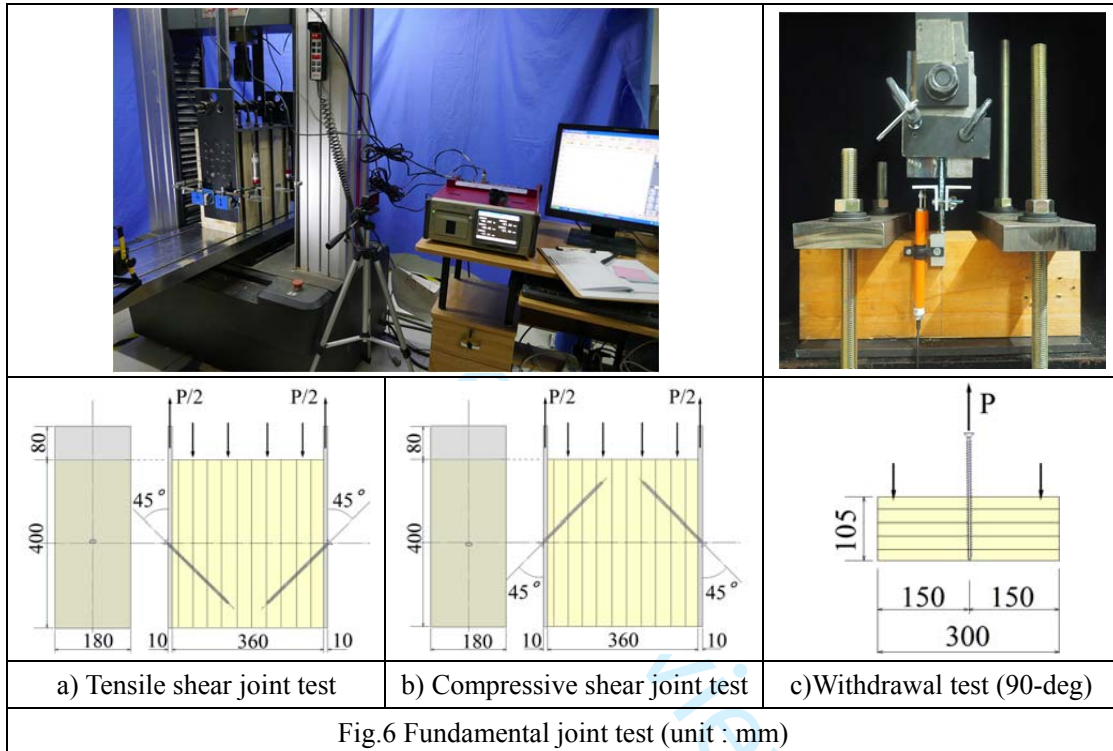
After the main experiments of the moment-resisting joint were finished, fundamental joint tests of STS were carried out using the same species of glulam, STS and steel plates used in the main experiments. Figures 6-a) to c) show the outline of the fundamental joint tests.

2.4.1 Fundamental Shear Joint Test on Inclined STS Glulam-Steel Plate Joint

One pair of symmetrically allocated 45-deg inclined STS was penetrated into glulam block through the 10 mm thick steel side plates having inclined lead-holes with 1 mm over-size than the outer diameter of the STS as shown in the photo of Fig.6-a) and b). Glulam block was fixed tightly to the steel base beam of the automatic electric testing machine (SUNSI—UTM5105:Max capacity of 150kN) using eight high strength steel rods. Pull load was given to the both steel side plates, so that a relatively stable shear loading condition was obtained. Load was measured by a load-cell (YBY-50kN) put on the crosshead. Relative slip deformations between glulam and steel plates were

1
2
3
4
5
6
7
8
9
10
11
12
13
14
15
16
17
18
19
20
21
22
23
24
25
26
27
28
29
30
31
32
33
34
35
36
37
38
39
40
41
42
43
44
45
46
47
48
49
50
51
52
53
54
55
56
57
58
59
60

1 measured using four deflection-measuring devices (YWC-100mm) set at four corners of the test
2 specimen. Load-slip relationships were recorded using a data logger (TDS-530). Crosshead speed
3 was 2 mm/min for all tests. Three replications were provided for these shear joint tests,
4 respectively.



6
7 **2.4.2 Withdrawal Test of STS Penetrated Perpendicular to the Grain of Glulam**
8 Withdrawal property of STS penetrated perpendicular to the grain of glulam was estimated using
9 Canadian spruce glulam made in Japan at Research Institute for Sustainable Humanosphere (RISH),
10 Kyoto University, Japan as shown in Fig.6-c) using a universal testing machine (INSTRON-100kN).
11 Load was measured by a load-cell (Instron-100kN) and withdrawal deflection was measured using
12 a pair of deflection measuring devices (CDPM-50mm). The load-deflection relationship was
13 recorded using a data logger (TDS-530). The penetrating depth of the STS was 95 mm (half of the
14 full length: 190 mm). Five replications were provided and cross head speed was 2 mm/min.

1
2
3
4
5
6
7
8
9
10
11
12
13
14
15
16
17
18
19
20
21
22
23
24
25
26
27
28
29
30
31
32
33
34
35
36
37
38
39
40
41
42
43
44
45
46
47
48
49
50
51
52
53
54
55
56
57
58
59
60

1 **3. Analyses**
2 **3.1 Mechanical Model**
3 **3.1.1 Assumption**

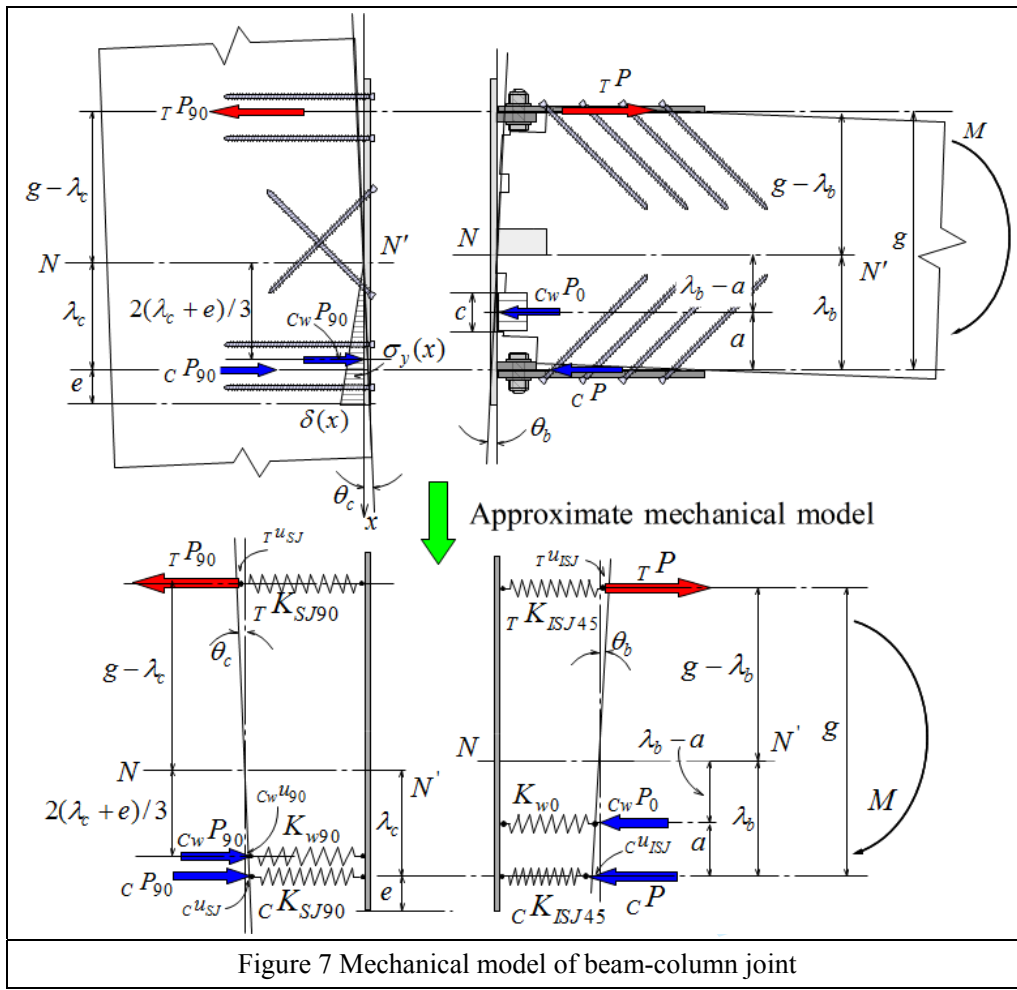


Figure 7 Mechanical model of beam-column joint

- 4
5 In this study, following assumptions were set out;
- 6 ● It will be the better to consider the effect of stiffness of steel base plate into the mechanical model, however, such approach will be quite sophisticate and make it difficult to solve nonlinear behavior by step-wise linear calculation method, therefore, in this study we selected an approximate mechanical model in which the steel base plate was assumed to behave like a rigid plate by neglecting its partial deflection as the “next best choice”.
 - 7
 - 8
 - 9
 - 10
 - 11 ● Judging from video observation on the experiments, contact at tensile and compressive sides

1
2
3
4
5
6
7
8
9
10
11
12
13
14
15
16
17
18
19
20
21
22
23
24
25
26
27
28
29
30
31
32
33
34
35
36
37
38
39
40
41
42
43
44
45
46
47
48
49
50
51
52
53
54
55
56
57
58
59
60

of the end-grain surface of beam to the steel base plate (length “c” in Fig.7) can be assumed as “even contact”, and that at the middle part of beam-end can be neglected.

- Contact of steel base plate to the side-grain surface of column can be assumed as “triangular rotational contact”, based on the preliminary analysis under the material constants and geometrical conditions given in this study.
- Effect of X-shaped STS on the moment resistance can be neglected.

Based on the above-mentioned assumption, a mechanical model of the beam-column joint was proposed as shown in Figure 7.

3.1.2 Location of the Neutral Axis at Beam-Side

The inclined screw groups inserting both in tensile and compressive sides have generalized Hooke’s laws shown in equations (1) and (2)

$$T P = T K_{ISJ45} \cdot T u_{ISJ} \dots (1)$$

$$C P = C K_{ISJ45} \cdot C u_{ISJ} \dots (2)$$

Relationships among the rotational angle, the distance from neutral axis to the axial forces and the corresponding deformations are given in equations (3) and (4).

$$T u_{ISJ} = (g - \lambda_b) \cdot \theta_b \dots (3)$$

$$C u_{ISJ} = \lambda_b \cdot \theta_b \dots (4)$$

Substituting equations (3) and (4) into (1) and (2), we get equations (5) and (6).

$$T P = T K_{ISJ45} \cdot (g - \lambda_b) \cdot \theta_b \dots (5)$$

$$C P = C K_{ISJ45} \cdot \lambda_b \cdot \theta_b \dots (6)$$

The compressive stress at end-grain surface of the beam can be assumed to be proportional to the compressive deformation via special embedment constant as shown in equation (7).

$$C_w \sigma = k_{w0} \cdot C_w u \dots (7)$$

1 The embedment coefficient of timber parallel to the grain k_{w0} is estimated by equation (8) in
2 accordance with AIJ standard (2009).

$$3 \quad k_{w0} = \frac{E_{w0}}{31.6 + 10.9 \cdot B_b} \dots (8)$$

4
5
6 A resultant compressive force due to “even contact” assumption is estimated in equation (9).

$$7 \quad c_w P_0 = c_w \sigma \times B_b \times c = (k_{w0} \cdot B_b \cdot c) \cdot c_w u = K_{w0} \cdot c_w u \dots (9)$$

8
9
10 The compressive resultant force, corresponding compressive deformation and geometrical
11 relationship for the “even contact” are consequently expressed in equation (10).

$$12 \quad c_w P_0 = K_{w0} \cdot c_w u$$

$$13 \quad c_w u = (\lambda_b - a) \cdot \theta_b \dots (10)$$

14
15 Taking the equilibrium equation among $T P$, $C P$ and $c_w P_0$, we obtain the location of neutral axis
16 in the beam-side joint as shown in equation (11).

$$17 \quad \lambda_b = \frac{T K_{ISJ45} \cdot g + K_{w0} \cdot a}{T K_{ISJ45} + C K_{ISJ45} + K_{w0}} \dots (11)$$

18
19
20 Taking the equilibrium equation among the internal moments and external moment, we can
21 obtain the rotational rigidity of beam-side joint as shown in equation (12).

$$22 \quad R_{Jb} = T K_{ISJ45} \cdot (g - \lambda_b)^2 + C K_{ISJ45} \cdot \lambda_b^2 + K_{w0} \cdot (\lambda_b - a)^2 \dots (12)$$

23 3.1.3 Location of the Neutral Axis on Column-Side Joint

24
25 STSs inserting perpendicular to the grain on both tensile and compressive side of the column
26 member have generalized Hooke’s laws shown in equations (13) and (14).
27
28

1
2
3
4
5
6
7
8
9
10
11
12
13
14
15
16
17
18
19
20
21
22
23
24
25
26
27
28
29
30
31
32
33
34
35
36
37
38
39
40
41
42
43
44
45
46
47
48
49
50
51
52
53
54
55
56
57
58
59
60

$$1 \quad {}_T P_{90} = {}_T K_{SJ90} \cdot {}_T u_{SJ} \dots (13)$$

$$2 \quad {}_C P_{90} = {}_C K_{SJ90} \cdot {}_C u_{SJ} \dots (14)$$

3

4 The resultant compressive force corresponding to the “triangular rotational contact” is derived as
5 shown in equation (15).

6

$$7 \quad {}_{C_w} P_{90} = B_s \cdot \int_0^{\lambda_c + e} \sigma(x) dx = \frac{B_s \cdot k_{w90} \cdot (\lambda + e)^2 \cdot \theta}{2} \dots (15)$$

8

9 Embedment coefficient of timber perpendicular to the grain k_{w90} is estimated by equation (16)
10 in accordance with AIJ standard (2009).

11

$$12 \quad k_{w90} = k_{w0} / 3.4, \quad k_{w0} = \frac{E_{w0}}{31.6 + 10.9 \cdot B_s} \dots (16)$$

13

14 Consequently, Hooke’s law for the compressive resultant force and corresponding compressive
15 deformation is expressed in equation (17).

16

$$17 \quad \left. \begin{aligned} {}_{C_w} P_{90} &= K_{w90} \cdot {}_{C_w} u \\ {}_{C_w} u &= \frac{2(\lambda_c + e)}{3} \cdot \theta \\ K_{w90} &= \frac{3B \cdot k_{w90} \cdot (\lambda_c + e)}{4} \end{aligned} \right\} \dots (17)$$

18

19 Taking the equilibrium equation among ${}_T P_{90}$, ${}_C P_{90}$ and ${}_{C_w} P_{90}$, we obtain the location of neutral
20 axis in the column-side joint as shown in equation (18).

21

$$22 \quad \lambda_c = \sqrt{\left(\frac{1}{B \cdot k_{w90}} \right)^2 ({}_C K_{SJ-90} + {}_T K_{SJ-90})^2 + \left(\frac{2}{B \cdot k_{w90}} \right) \cdot [{}_T K_{SJ-90} \cdot (e + g) + {}_C K_{SJ-90} \cdot e]} - \left[\frac{1}{B \cdot k_{w90}} \cdot ({}_C K_{SJ-90} + {}_T K_{SJ-90}) \right] \dots (18)$$

23

24 Taking the equilibrium equation between the internal moments and external moment, we can

1 obtain the rotational rigidity of column-side joint as shown in equation (19).

$$R_{Jc} = T K_{SJ-90} \cdot (g - \lambda_c)^2 + C K_{SJ-90} \cdot \lambda_c^2 + \frac{B \cdot k_{w90} \cdot (\lambda_c + e)^3}{3} \dots (19)$$

3.1.4 Total Rotational Rigidity of Beam-Column Joint

The total rotational angle between beam and column is a sum of the each rotational angle, hence

$$\theta = \theta_b + \theta_c = \frac{M}{R_{Jb}} + \frac{M}{R_{Jc}} = \left(\frac{1}{R_{Jb}} + \frac{1}{R_{Jc}} \right) \cdot M = \frac{M}{R_{Jbc}} \dots (20)$$

$$R_{Jbc} = \left(\frac{R_{Jb} \cdot R_{Jc}}{R_{Jb} + R_{Jc}} \right) \dots (21)$$

3.2 Hysteresis Loop

Hysteresis loops of MRJ specimens were approximated by the Normalized Characteristic Loop (NCL) model which was originally proposed by Tani et al. (1972) for expressing hysteresis loops of reinforce concrete structures. Recently, Matsunaga et al. (2009) extended NCL-model successfully also to the wooden post and beam shear wall structures. They proposed the functions to be used in the extended NCL-model as shown in equation (22).

$$\left. \begin{aligned} \text{Upper loading : } {}_U L(x)_L &= [B \cdot |x|^{n1} + 1 - B]x - A(x^4 - 1) \quad \dots(a) \\ \text{Lower unloading : } {}_L L(x)_{UL} &= [B \cdot |x|^{n2} + 1 - B]x + A(x^4 - 1) \quad \dots(b) \\ \text{Lower loading : } {}_L L(x)_L &= [B \cdot |x|^{n1} + 1 - B]x + A(x^4 - 1) \quad \dots(c) \\ \text{Upper unloading : } L(x)_{UL} &= [B \cdot |x|^{n2} + 1 - B]x - A(x^4 - 1) \quad \dots(d) \end{aligned} \right\} \dots (22)$$

where,

$L(x)$: Normalized load divided by the peak value in each loop

x : Normalized deformation divided by peak value in each loop

1
2
3
4
5
6
7
8
9
10
11
12
13
14
15
16
17
18
19
20
21
22
23
24
25
26
27
28
29
30
31
32
33
34
35
36
37
38
39
40
41
42
43
44
45
46
47
48
49
50
51
52
53
54
55
56
57
58
59
60

Figure 8 shows examples of normalized loops described based on the rules of extended NCL-model. Parameter “A” indicates the values of P/P_{max} at $x=0$. In the case of different peak values P_{max} at loading-side and unloading-side, continuities of loop at $x=0$ cannot be ensured. Therefore, in this study, parameter “A” was first determined so as to fit the whole closed loop, afterward unloading-side A was adjusted to make the continuity of P-values at $x=0$ held.

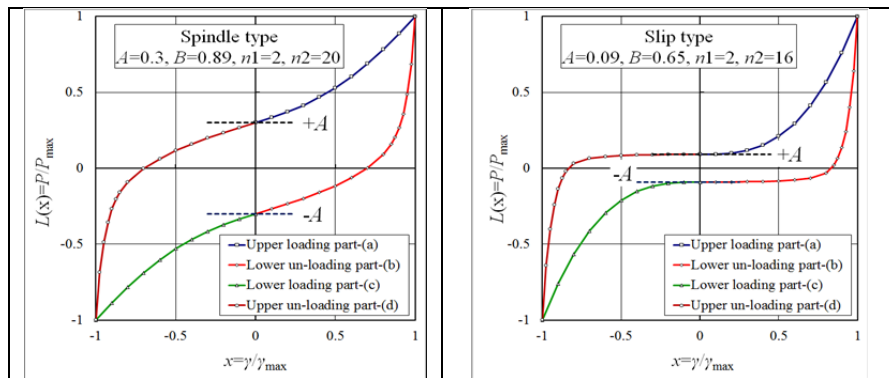
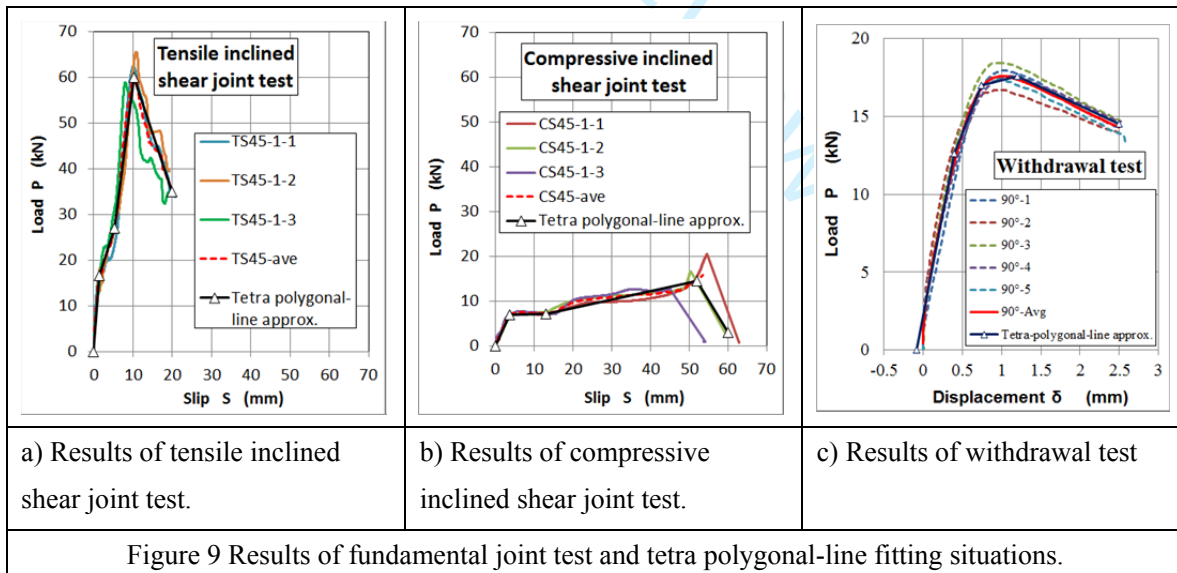


Figure 8: Typical loops drawn based on the rule of the extended NCL-model

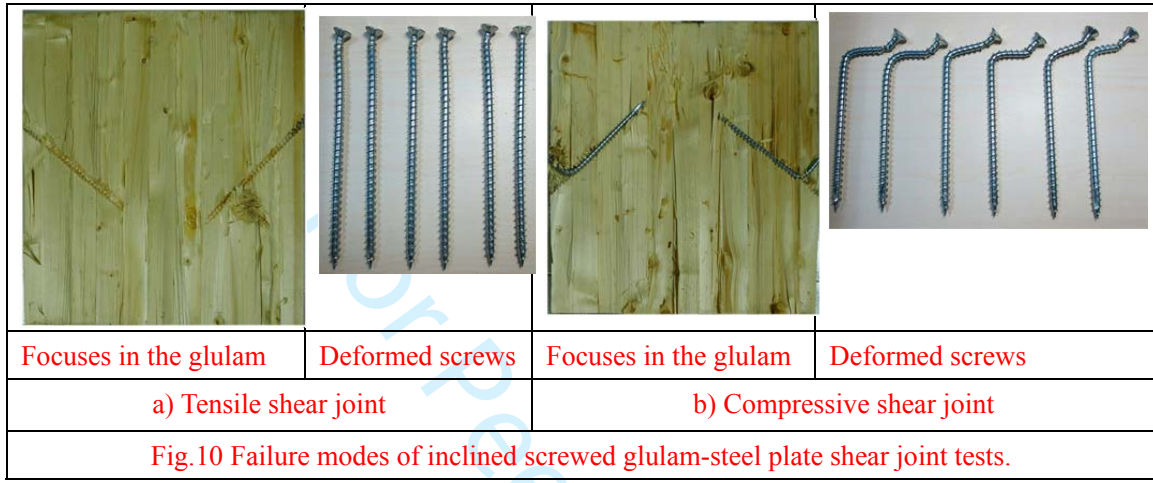
4. Results and Discussion

4.1 Results of Fundamental Joint Tests



1
2
3
4
5
6
7
8
9
10
11
12
13
14
15
16
17
18
19
20
21
22
23
24
25
26
27
28
29
30
31
32
33
34
35
36
37
38
39
40
41
42
43
44
45
46
47
48
49
50
51
52
53
54
55
56
57
58
59
60

1 Figures 9-a) and b) show the results of fundamental shear joint tests on the inclined STS joint
2 and Fig. 9-c) shows the results of withdrawal test of STS penetrated perpendicular to the grain of
3 glulam.
4



5
6 Figures 10-a) and b) show the failure modes of tensile shear joint and compressive shear joint,
7 respectively. From Fig.9-a) and Fig.10-a), it is clear that STS did not deform so much and was
8 likely to be pulled out relatively smoothly in the case of tensile shear joint. The first slightly
9 crooked point at about 17kN in Fig.9-a) might correspond to a small scale bending at about 1/3 to
10 1/4 point of shank from the screw head, afterwards monotonic pullout was likely to be kept until
11 the maximum load. On the other hand, from Fig.9-b) and Fig.10-b), it is clear that STS deformed
12 remarkably in the case of compressive shear joint. The first clear crooked point at about 7kN in
13 Fig.9-b) might correspond to the fatal bending at about 1/4 point of shank from the screw head,
14 afterwards the second bending might occur at the point closer to the screw head, which might
15 correspond to the final load rising before the maximum load. In the case of withdrawal test, typical
16 smooth pullout behavior was observed as can be seen from Fig.9-c).

17 For predicting the skeleton curve of the moment-rotational relationships of the full-scale
18 beam-column joint specimens, data obtained by the fundamental joint tests were approximated by
19 tetra polygonal-lines as shown in Fig.9 (solid lines with markers). Tables 2 to 4 show parameters
20 compose of each tetra polygonal-line with which stepwise linear calculations are to be executed in
21 the section 4.2.
22

1 Table 2 Parameters of the tetra polygonal-line approximation for the tensile inclined shear joint

Fundamental tensile shear joint specimen composed of 2rows-1line STS				Tensile shear joint composed of 2rows-4lines STS in the full-scale moment-resisting joint		
Boundary point	Slip <i>S</i>	Load <i>P</i>	Stiffness <i>K</i>	Slip <i>S</i>	Total Load $P_n = P \times n_{ef}$	Stiffness <i>K</i>
<i>i</i>	mm	kN	kN/mm	mm	kN	kN/mm
	0.00	0.00		0.00	0.00	
1	1.40	16.52	11.80	1.40	57.52	41.08
2	5.40	27.00	2.62	5.40	94.02	9.13
3	10.20	60.00	6.88	10.20	208.93	23.94
4	20.00	35.00	-2.55	20.00	121.88	-8.88

2 Remark: $n=4$, $n_{ef} = (n)^{0.9} = (4)^{0.9} = 3.482$ (in accordance with EC-5 (2008))

3
4 Table 3 Parameters of the tetra polygonal-line approximation for the compressive inclined shear joint

Fundamental tensile shear joint specimen composed of 2rows-1line STS				Compressive shear joint composed of 2rows-4lines STS in the full-scale moment-resisting joint		
Boundary point	Slip <i>S</i>	Load <i>P</i>	Stiffness <i>K</i>	Slip <i>S</i>	Total Load $P_n = P \times n_{ef}$	Stiffness <i>K</i>
<i>i</i>	mm	kN	kN/mm	mm	kN	kN/mm
	0.00	0.00		0.00	0.00	
1	3.60	6.90	1.92	3.60	24.03	6.67
2	13.00	7.10	0.02	13.00	24.72	0.07
3	52.00	14.50	0.19	52.00	50.49	0.66
4	60.00	3.00	-1.44	60.00	10.45	-5.01

5 Remark: $n=4$, $n_{ef} = (n)^{0.9} = (4)^{0.9} = 3.482$ (in accordance with EC-5 (2008))

6
7 Table 4 Parameters of the tetra polygonal-line approximation for the withdrawal behavior of STS

Fundamental withdrawal specimen composed of 1rows-1line STS penetrating half length				Tensile joint composed of 2rows-4lines full length STS in the full-scale moment-resisting joint		
Boundary point	Slip <i>S</i>	Load <i>P</i>	Stiffness <i>K</i>	Slip <i>S</i>	Total Load $P_n = P \times n_{ef} \times 2$	Stiffness <i>K</i>
<i>i</i>	mm	kN	kN/mm	mm	kN	kN/mm
	-0.08	0.00		0	0	
1	0.40	12.60	26.25	0.40	163.75	409.38
2	0.74	17.00	12.94	0.74	220.93	168.18
3	1.20	17.60	1.30	1.20	228.73	16.95
4	2.50	14.50	-2.38	2.50	188.44	-30.99

8 Remarks on P_n : $n=8$, $n_{ef} = (n)^{0.9} = (8)^{0.9} = 6.5$ (in accordance with EC-5 (2008)).

9
10 In each table, left-hand side columns indicate the basic values estimated by the fundamental

1 shear joint tests, and the right-hand side ones correspond to the performance of the actual joints in
2 the full-scale specimen evaluated by considering the effective numbers n_{ef} (EC-5, 2008) of STS. As
3 a common remark for these three tables, “boundary point” means the four points consisting of each
4 tetra polygonal-line. In the Table 4, the reason why “total load” is multiplied by 2 is that the
5 penetration depth of full-threaded STS in the fundamental withdrawal tests was half of the full
6 effective length.

7 For the partial embedment of glulam, we assumed that stress (σ) - deformation (u) relationship of
8 the embedment on the glulam surface had a bilinear form in which initial slope was estimated by
9 equations (8) or (16) and the secondary slope was estimated as 1/8 of the initial slope in accordance
10 with the empirical rule used in the standard (AIJ standard, 2009). Only the push-in capacity of STS
11 was not evaluated by the experiment but it was assumed to be the same as that of withdrawal
12 capacity in accordance with the suggestion of Bejtka & Blaß (2006) except for the final
13 load-decreasing region. In this study, as a kind of “spring-back effect” was expected in some extent
14 if the partial compression region has sufficient end-distance, therefore, we assumed that the load
15 would be kept as it is for meanwhile after maximum load.

16 4.2 Calculation Methods

17 4.2.1 Calculation of the skeleton curve

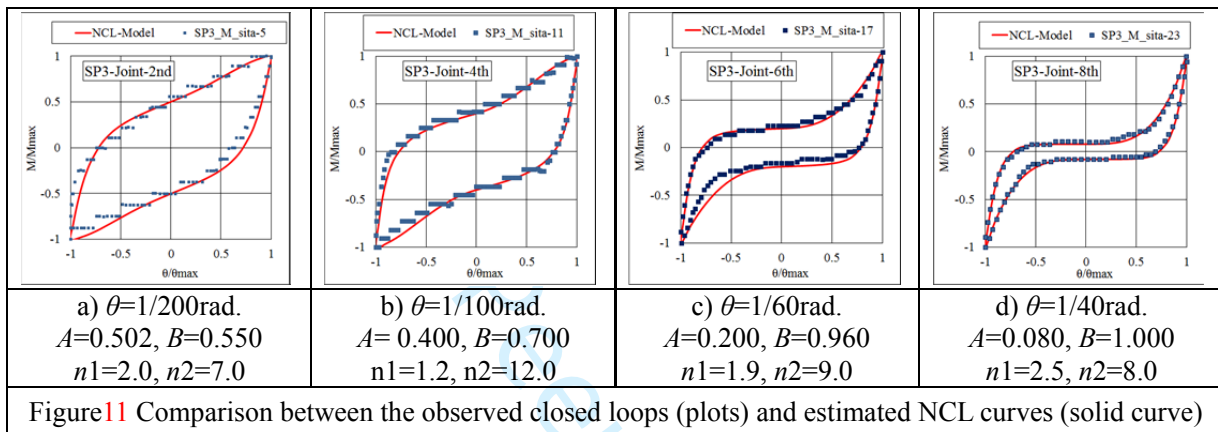
18 Stepwise linear calculations for predicting the skeleton curves were done using the rotational
19 angle increment of 0.0001 rad. based on the equations shown in the section 3.1. In each incremental
20 step, all deformations corresponding to the moment-resisting components were checked whether
21 they exceeded the “boundary point” values shown in Tables 3 to 5. If some deformation exceeded
22 i -th “boundary point”, i -th stiffness was replaced by $i+1$ -th stiffness afterward the location of the
23 neutral axis and the total resisting-moment were re-calculated. This calculation process repeated
24 until the maximum target rotational angle.

25 4.2.2 Analyses on the observed loops for estimating NCL parameters

26 In order to estimate the parameters for the extended NCL model, moment-rotational angle data
27 observed in the full-scale experiments were analyzed and divided into individual 34 closed loops
28 (11 steps \times 3 repeated cycles + last return loop) in each specimen. NCL parameters were identified
29 using the second cyclic data of each three cyclic loops because the first cyclic data involved partly
30 skeleton curve data. Figures 11-a) to d) show a several comparison between the observed closed
31
32

1 loops (blue plots) and estimated NCL curves (solid red-curve).

2 It can be seen from Fig.11 that hysteresis loop gradually changes from the spindle shape to the
3 slip or/and pinching shape as the rotational angle increases. In this study, discrete values of NCL
4 parameters estimated by the above mentioned loop analyses were directly used in the calculations
5 for predicting hysteresis loops of the moment-rotational angle relationships.



4.2.3 Calculation of hysteresis loops combined with skeleton curve data

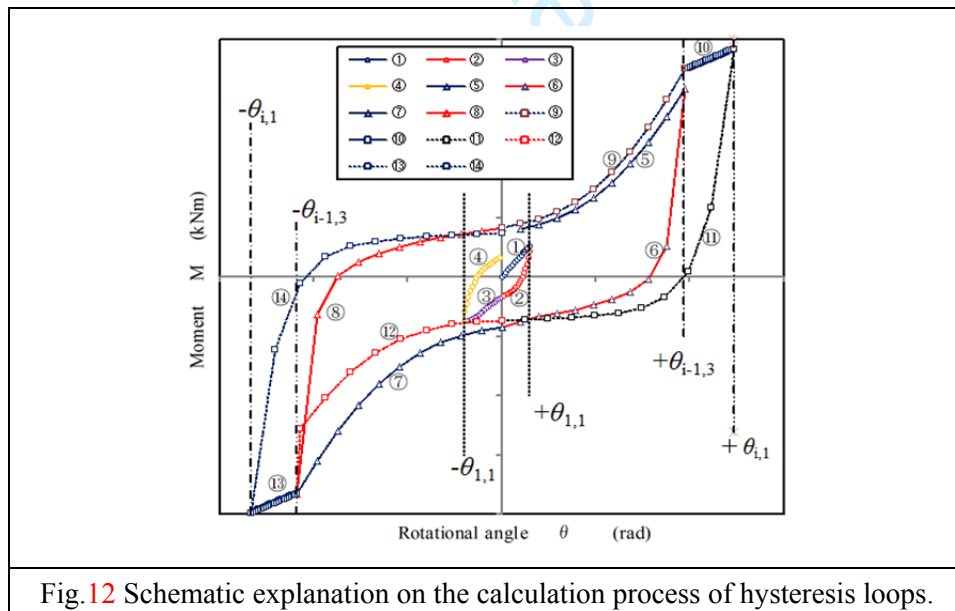


Figure 12 explains the calculation process of hysteresis loops. The circled number put near the plots in Fig.12 corresponds to those put in front of the following equations. Alphabets put after the equations correspond to those in equation (22). In the first cycle of any steps, “Skeleton Curve Data” obtained theoretically in the section 4.2.1 is to be used partly or in the whole.

(First cycle of the first step)

① $0 \leq \theta \leq \theta_{1,1}$: $M = F(0) \rightarrow M = F(\theta_{1,1})$: Follows on the “Skeleton Curve Data”

② $\theta_{1,1} \geq \theta \geq 0$: Lower unloading: $M = \left[\left\{ B_1 \cdot \left| \frac{\theta}{\theta_{1,1}} \right|^{n_{2,1}} + 1 - B_1 \right\} \left(\frac{\theta}{\theta_{1,1}} \right)^{+A_1} \left\{ \left(\frac{\theta}{\theta_{1,1}} \right)^4 - 1 \right\} \right]_m^+ M_{1,1} \dots$ (b)

③ $0 \geq \theta \geq -\theta_{1,1}$: Lower loading: $M = \left[\left\{ B_1 \cdot \left| \frac{\theta}{-\theta_{1,1}} \right|^{n_{1,1}} + 1 - B_1 \right\} \left(\frac{\theta}{-\theta_{1,1}} \right)^{-A_1} \left\{ \left(\frac{\theta}{-\theta_{1,1}} \right)^4 - 1 \right\} \right]_m^- M_{1,1} \dots$ (c)

④ $-\theta_{1,1} \leq \theta \leq 0$: Upper unloading: $M = \left[\left\{ B_1 \cdot \left| \frac{\theta}{-\theta_{1,1}} \right|^{n_{2,1}} + 1 - B_1 \right\} \left(\frac{\theta}{-\theta_{1,1}} \right)^{-A_1} \left\{ \left(\frac{\theta}{-\theta_{1,1}} \right)^4 - 1 \right\} \right]_m^- M_{1,1} \dots$ (d)

(3rd cycle of $i-1$ th step)

⑤ $0 \leq \theta \leq \theta_{i-1,3}$: Upper loading: $M = \left[\left\{ B_{i-1} \cdot \left| \frac{\theta}{\theta_{i-1,3}} \right|^{n_{1,i-1}} + 1 - B_{i-1} \right\} \left(\frac{\theta}{\theta_{i-1,3}} \right)^{-A_{i-1}} \left\{ \left(\frac{\theta}{\theta_{i-1,3}} \right)^4 - 1 \right\} \right]_m^+ M_{i-1,3} \dots$ (a)

⑥ $\theta_{i-1,3} \geq \theta \geq 0$: Lower unloading: $M = \left[\left\{ B_{i-1} \cdot \left| \frac{\theta}{\theta_{i-1,3}} \right|^{n_{2,i-1}} + 1 - B_{i-1} \right\} \left(\frac{\theta}{\theta_{i-1,3}} \right)^{+A_{i-1}} \left\{ \left(\frac{\theta}{\theta_{i-1,3}} \right)^4 - 1 \right\} \right]_m^+ M_{i-1,3} \dots$ (b)

⑦ $0 \geq \theta \geq -\theta_{i-1,3}$: Lower loading: $M = \left[\left\{ B_{i-1} \cdot \left| \frac{\theta}{-\theta_{i-1,3}} \right|^{n_{1,i-1}} + 1 - B_{i-1} \right\} \left(\frac{\theta}{-\theta_{i-1,3}} \right)^{-A_{i-1}} \left\{ \left(\frac{\theta}{-\theta_{i-1,3}} \right)^4 - 1 \right\} \right]_m^- M_{i-1,3} \dots$ (c)

⑧ $-\theta_{i-1,3} \leq \theta \leq 0$: Upper unloading: $M = \left[\left\{ B_{i-1} \cdot \left| \frac{\theta}{-\theta_{i-1,3}} \right|^{n_{2,i-1}} + 1 - B_{i-1} \right\} \left(\frac{\theta}{-\theta_{i-1,3}} \right)^{-A_{i-1}} \left\{ \left(\frac{\theta}{-\theta_{i-1,3}} \right)^4 - 1 \right\} \right]_m^- M_{i-1,3} \dots$ (d)

(1st cycle of i th step)

⑨ $0 \leq \theta \leq \theta_{i-1,3}$: Upper loading: $M = \left[\left\{ B_{i-1} \cdot \left| \frac{\theta}{\theta_{i-1,3}} \right|^{n_{1,i-1}} + 1 - B_{i-1} \right\} \left(\frac{\theta}{\theta_{i-1,3}} \right)^{-A_{i-1}} \left\{ \left(\frac{\theta}{\theta_{i-1,3}} \right)^4 - 1 \right\} \right]_m^+ M_{i-1,3} \dots$ (a)

⑩ $\theta_{i-1,3} \leq \theta \leq \theta_{i,1} : M = F(\theta_{i-1,3}) \rightarrow M = F(\theta_{i,1})$: Follows on the “Skeleton Curve Data”

⑪ $\theta_{i,1} \geq \theta \geq 0$: Lower unloading:
$$M = \left[\left\{ B_i \cdot \left| \frac{\theta}{\theta_{i,1}} \right|^{n_{2i}} + 1 - B_i \right\} \left(\frac{\theta}{\theta_{i,1}} \right)^{+A_i} \left\{ \left(\frac{\theta}{\theta_{i,1}} \right)^4 - 1 \right\} \right] \cdot {}^+M_{i,1} \dots \text{(b)}$$

⑫ $0 \geq \theta \geq -\theta_{i-1,3}$: Lower loading:
$$M = \left[\left\{ B_i \cdot \left| \frac{\theta}{-\theta_{i,1}} \right|^{n_1} + 1 - B_i \right\} \left(\frac{\theta}{-\theta_{i,1}} \right)^{-A_i} \left\{ \left(\frac{\theta}{-\theta_{i,1}} \right)^4 - 1 \right\} \right] \cdot {}^-M_{i,1} \dots \text{(c)}$$

⑬ $-\theta_{i-1,3} \geq \theta \geq -\theta_{i,1} : M = F(-\theta_{i-1,3}) \rightarrow M = F(-\theta_{i,1})$: Follows on the “Skeleton Curve Data”

⑭ $-\theta_{i,1} \leq \theta \leq 0$: Upper unloading:
$$M = \left[\left\{ B_i \cdot \left| \frac{\theta}{-\theta_{i,1}} \right|^{n_{2i}} + 1 - B_i \right\} \left(\frac{\theta}{-\theta_{i,1}} \right)^{-A_i} \left\{ \left(\frac{\theta}{-\theta_{i,1}} \right)^4 - 1 \right\} \right] \cdot {}^-M_{i,1} \dots \text{(d)}$$

where,

$F(\theta)$: Theoretical moment M as the function of rotational angle θ (Skeleton Curve Data)

$\pm\theta_{i,j}$: Assigned or observed peak value (plus or minus) of θ on j^{th} -cycle of i^{th} -step

${}^+M_{i,j}$: Theoretical **loading**-side peak value (maximum) of M on j^{th} -cycle of i^{th} -step

${}^-M_{i,j}$: Theoretical **unloading**-side peak value (minimum) of M on j^{th} -cycle of i^{th} -step

${}^-A_i = {}^+A_i \cdot \left(\frac{{}^+M_{i,j}}{{}^-M_{i,j}} \right)$: A -value adjusted so as to hold the continuity of M -values at $x=0$ on j^{th} -cycle of i^{th} -step

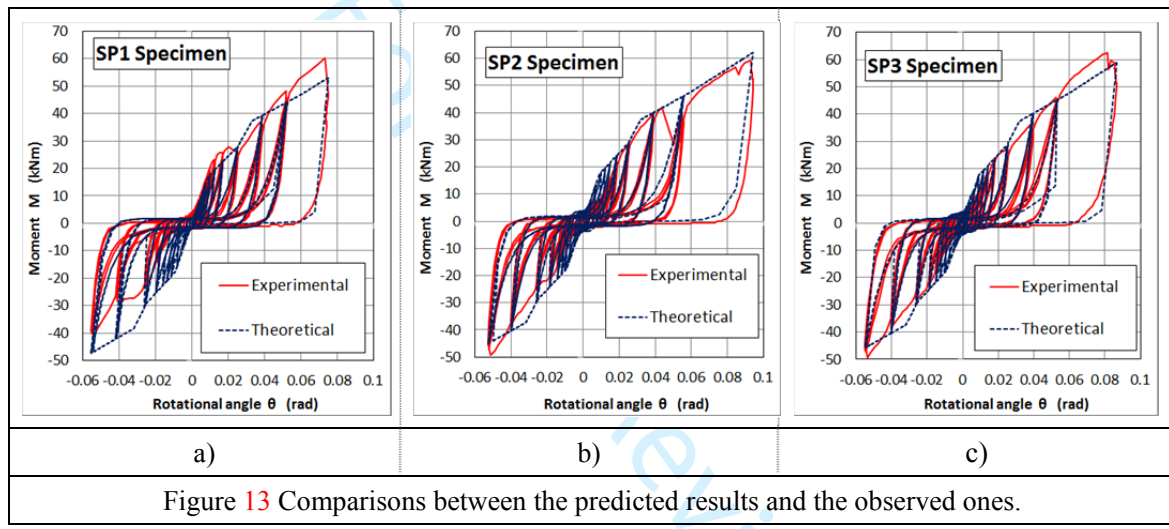
4.3 Results of Hysteresis Loops Predicted with Theoretical Skeleton Curve Data

Figures 13-a) to c) show comparisons between predicted results (dotted line) and observed ones (solid line). On the whole, agreements between predictions and observations seem good. The extended NCL model could give better predictions for the nonlinear behaviors of glulam moment-resisting joint specimens subject to static push-pull cyclic load. In the SP1 specimen, however, some extent of discrepancy between predictions and observations was observed in push region (minus region). This reason is not clear rigorously but a few errors on the setting of vertical location of loading jig and a miss loading till 1/100 rad. before the formal experiment might have effects on these errors.

Throughout three test results shown in Figs13-a) to c), it was confirmed that there were a few

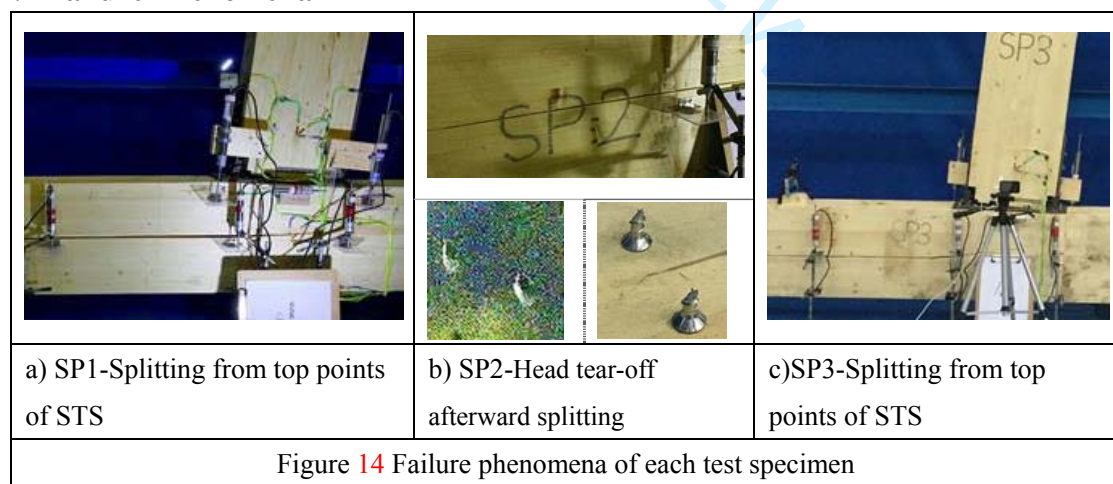
1
2
3
4
5
6
7
8
9
10
11
12
13
14
15
16
17
18
19
20
21
22
23
24
25
26
27
28
29
30
31
32
33
34
35
36
37
38
39
40
41
42
43
44
45
46
47
48
49
50
51
52
53
54
55
56
57
58
59
60

1 crooking points on the moment-rotational angle skeleton curves. According to our analyses, the first
2 yielding moment at around 17kNm was brought mainly by the first crooking point of both
3 tensile-inclined STS joint and compressive inclined STS joint in the beam-side joint. The second one
4 at around 38kN was brought by the second crooking point of both compressive inclined STS joint and
5 yielding of end-grain surface beam member. Consequently, no pullout failure from tensile inclined
6 STS joint occurred within the material properties and geometrical conditions provided in these
7 experiments.



9
10

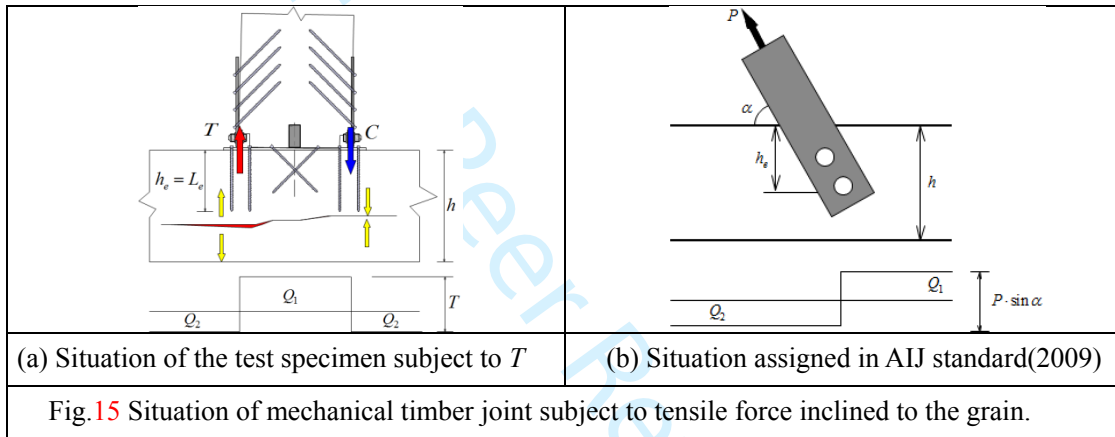
4.4 Failure Phenomena



1
2
3
4
5
6
7
8
9
10
11
12
13
14
15
16
17
18
19
20
21
22
23
24
25
26
27
28
29
30
31
32
33
34
35
36
37
38
39
40
41
42
43
44
45
46
47
48
49
50
51
52
53
54
55
56
57
58
59
60

1 Figures 14-a) to c) show failure phenomena of each test specimen. All specimens finally failed
2 by splitting of column member which seemed to start from the top-point of tensile STSs penetrated
3 perpendicular to the grain of column member.

4 Only on the SP2 specimen, heads of two screws were first torn off at about 1/20 rad. as shown in
5 the lower photos in Fig.14-b), afterward splitting failure occurred quite the same as the cases in
6 other two specimens. This kind of splitting failure might be understood as a result due to the
7 stronger multiple STSs joint against the weaker timber load carrying capacity that is similar to the
8 situation of tensile mechanical joint loaded inclined to the grain direction.



10 Figure 15-(a) illustrates the situation occurred in the moment-resisting joint specimen subject to
11 the tensile force T perpendicular to the grain. While Fig.15-(b) shows a mechanical joint subject to
12 α -degree inclined tensile force P to the grain direction that is assigned in the AIJ standard (2009),
13 and equations 23-(a) to (d) give predictions for the ultimate load carrying capacity P .

14
15

$$\begin{aligned}
 P_{uw} &= \min(P_{uw1}, P_{uw2}) & (a) \\
 P_{uw1} &= \left(\frac{2 \cdot C_r \cdot l}{\sin \alpha} \right) \sqrt{\frac{h_e}{1 - \frac{h_e}{h}}} & (b) \\
 P_{uw2} &= \frac{2 \cdot \xi \cdot h_e \cdot l \cdot F_s}{3 \sin \alpha} & (c) \\
 \xi &= \frac{Q_1 + Q_2}{\max(|Q_1|, |Q_2|)} & (d)
 \end{aligned}
 \quad \left. \vphantom{\begin{aligned} P_{uw} \\ P_{uw1} \\ P_{uw2} \\ \xi \end{aligned}} \right\} \dots(23)$$

The C_r can be estimated by equation (24) via specific gravity of material (AIJ standard, 2009).

$$C_r = 39.6 \cdot r_0 - 4.44 \dots(24)$$

Considering the geometrical size of the beam-column joint specimen (L is column length of 3m, h_b is beam depth of 0.362m) as well as material constants, equations (23) and (24) gave the following results;

$$\xi = \frac{Q_1 + Q_2}{\max(|Q_1|, |Q_2|)} = \frac{Q_2 \left(\frac{L}{h_b} - 1 \right) + Q_2}{Q_2 \left(\frac{L}{h_b} - 1 \right)} = 1.137$$

$$P_{uw1} = \left(\frac{2 \cdot C_r \cdot l}{\sin \alpha} \right) \sqrt{\frac{h_e}{1 - \frac{h_e}{h}}} = \{2 \times (39.6 \times 0.449 - 4.44) \times 180\} \sqrt{\frac{200 - 10}{1 - \frac{200 - 10}{360}}} = 96.33 \text{ kN}$$

$$P_{uw2} = \frac{2 \cdot \xi \cdot h_e \cdot l \cdot F_s}{3 \sin \alpha} = \frac{2 \times 1.137 \times (200 - 10) \times 180 \times 6.2}{3} = 160.76 \text{ kN}$$

$$P_{uw} = \min(P_{uw1}, P_{uw2}) = \min(96.33, 160.76) = 96.33 \text{ kN} = T \quad (\text{Refer to the Fig.15-a) for "T"})$$

While the incremental step-wise linear calculation in the section 4.2.1 gave a regression equation between moment M and tensile force T as $M=0.5233 \times T$. From this equation, the moment at $T=96.33 \text{ kN}$ was predicted as $M_{\text{-predict}}=0.5233 \times 96.33 = 50.38 \text{ kNm}$. On the other hand, observed maximum moments were $M_{\text{-obs1}}=49.06 \text{ kNm}$, $M_{\text{-obs2}}=48.20 \text{ kNm}$, $M_{\text{-obs3}}=50.80 \text{ kNm}$ and average

1 value was $M_{\text{obs-ave}}=49.35\text{kNm}$. Therefore, theoretical prediction gave almost the same value as that
2 of observed $M_{\text{predict}}/M_{\text{obs-ave}}=50.38/49.35=1.02$.

3 4 **5. Conclusions**

5 This study aimed to predict nonlinear behaviors of glulam beam-column MRJ specimens based
6 on the mechanical model for the skeleton curve and the extended NCL model for hysteresis loops.
7 From the comparisons between experimental **results of three replications** and **analytical** results, the
8 following points were concluded:

- 9
- 10 ● The tensile shear joint consisted of glulam and steel side plate with inclined STS showed
11 excellent initial stiffness and maximum load carrying capacity with less ductility. On the other
12 hand, the compressive shear joint consisted of glulam and steel side plate with inclined STS
13 showed inferior initial stiffness and maximum load carrying capacity with better deformability
14 compared with tensile joint.
 - 15 ● Moment-rotational behaviors of the test specimen showed typical slip-type hysteresis loop as
16 the rotational angle increased.
 - 17 ● The skeleton curve of the specimens could be predicted well by the incremental step-wise
18 linear calculation method, in which load-deformation relationships of all moment-resisting
19 components were assumed by tetra polygonal-lines or/and bi-linear lines.
 - 20 ● Extended NCL hysteresis model of each test specimen was consisted of parameters identified
21 from the second cycle data of the each step observed in the experiments. Combining with the
22 theoretical skeleton curve data, the whole nonlinear behaviors of the test specimens could be
23 described well similar to those of observed.
 - 24 ● Maximum load carrying capacities of test specimens could be predicted well by applying the
25 design equations for the tensile mechanical joint loaded with inclination to the grain direction.

26 27 **Acknowledgements**

28 Full-threaded STS used in this research were all donated by Rothoblass®, Italy. Authors would
29 like to express their sincere thanks to this support.

30 31 **Declaration of Conflicting Interests**

32 The authors declared no potential conflicts of interest with respect to the research, authorship,

1
2
3
4
5
6
7
8
9
10
11
12
13
14
15
16
17
18
19
20
21
22
23
24
25
26
27
28
29
30
31
32
33
34
35
36
37
38
39
40
41
42
43
44
45
46
47
48
49
50
51
52
53
54
55
56
57
58
59
60

1 and/or publication of this article.

2

3 **Funding**

4 This work was supported by the Special Fund for National Natural Science Foundation of China
5 [Project No.31670566]

6

7 **References**

8 AIJ standard (2009), Architectural Institute of Japan (edited) Chapter 6, Design of joint; p.164; in
9 Standard for Structural Design of Timber Structures, (in Japanese), Forth edition; 2nd print,
10 Maruzen.
11 Bejtka I, Blaß HJ (2002) Joints with inclined screws. In: Proc. of the CIB-W18 Meeting 35, Paper
12 No.CIB-W18/35-7-5, Kyoto, Japan.
13 Bejtka I, Blaß HJ (2005) Self-Tapping-Screws as Reinforcements in Connections with Dowel-Type
14 Fastener. In: Proc. of the CIB-W18 Meeting 38, Paper No. CIB-W18/38-7-4, Karlsruhe,
15 Germany.
16 Bejtka I, Blaß HJ (2006) Self-Tapping-Screws as Reinforcements in Beam Supports. In: Proc. of
17 the CIB-W18 Meeting 39, Paper No. CIB-W18/39-7-4, 2006, Florence, Italy.
18 Blaß HJ, Bejtka I (2001) Screws with continuous threads in timber connection. In: Proceedings
19 PRO 22: International RILEM Symposium on Joints in Timber Structures, Stuttgart, Germany;
20 193-201
21 Blaß HJ, Bejtka I (2004) Reinforcements perpendicular to the grain using self-tapping screws. In:
22 Proceedings of WCTE2004 :1001-1006, Lahti, Finland.
23 Blaß HJ, Schmid M (2001) Self-tapping screws as reinforcement perpendicular to the grain in
24 timber connections, In: Joints in Timber Structures. Proceedings of the International RILEM
25 Symposium, RILEM Publications S.A.R.L. Stuttgart, Germany.
26 Brandner R, Ringhofer A, Grabner M (2018) Probabilistic Models for the Withdrawal Behavior of
27 Single Self-Tapping Screws in the Narrow Face of Cross Laminated Timber, European Journal
28 of Wood Products 76:13–30.
29 Buchanan AH, Fairweather RH (1993) Seismic design of glulam structures. Bulletin of the NZ
30 Society for the Earthquake Engineering 26(4): 415-436.
31 [http://www.nzsee.org.nz/db/Bulletin/Archive/26\(4\)0415.pdf](http://www.nzsee.org.nz/db/Bulletin/Archive/26(4)0415.pdf) (Accessed on 2018.11.26)
32 EC-5 (2008) : CEN: EN 1995-1-1/A1, Eurocode 5: Design of timber structures - Part 1-1: General

- 1
2
3
4
5
6
7
8
9 1 – Common rules and rules for buildings. European Committee for Standardization CEN,
10 Bruxelles, Belgium
11 2
12 3 Frese M, Blaß HJ (2009) Models for the Calculation of the Withdrawal Capacity of Self-tapping
13 Screws, In: Proc. of the CIB-W18 Meeting 42, Paper No. CIB-W18/42-7-3, Dübendorf,
14 Switzerland.
15 5
16 6 GB/T 1933-2009 (2009) Method for determination of the density of wood (in Chinese). Standards
17 Press of China, Beijing, China.
18 7
19 8 GB/T 26899-2011 (2011) Structural glued laminated timber (in Chinese). Standards Press of China,
20 Beijing, China.
21 9
22 10 GB/T 50329-2012 (2012) Standard for test methods of timber structures (in Chinese).China
23 Building Industry Press, Beijing, China.
24 11
25 12 Girhammar UA, Jacquier N, Källsner B (2017) Stiffness Model for Inclined Screws in
26 Shear-Tension Mode in Timber-to-Timber Joints, Engineering Structures ;136:580-595.
27 13
28 14 Hübner U, Rasser M, Schickhofer G (2010) Withdrawal capacity of screws in European ash
29 (fraxinus excelsior) In: Proceedings of WCTE2010, (CD-ROM), Riva del Garda, Trentino,
30 Italy.
31 16
32 17 Japan Housing and Wood Technology Center (2008) Allowable stress design method for wooden
33 post-and-beam constructions 2008 version (in Japanese); Chapter 6, 4thprint, Tokyo.
34 18
35 19 Jockwer R, Steiger R, Frangi A (2014) Design model for inclined screws under varying load to
36 grain angles, International Network on Timber Engineering Research, INTER/47-7-5, 1st
37 INTER Meeting, 01 to 04 September, Bath, United Kingdom.
38 21
39 22 Kevarinmäki A (2002) Joints with inclined screws. In: Proc. of the CIBW-18 Meeting 35, Paper No.
40 CIB-W18/35-7-4, Kyoto, Japan.
41 23
42 24 Komatsu K, Kawamoto N, Horie K, Harada M (1991) Modified glulam moment-resisting joints. In:
43 Proceedings 1991 International Timber Engineering Conference London, 3: 3.111-3.118,
44 London, UK.
45 26
46 27 Komatsu K (2017) Development of stiffer and ductile glulam portal frame, In Proceedings of the
47 3rd International Conference on Construction and Building Engineering (ICONBUILD), AIP
48 Conf. Proc. 1903, 020026-1–020026-15; <https://doi.org/10.1063/1.5011506> (Accessed on
49 2018.11.26)
50 29
51 30
52 31 Krenn H, Schickhofer G (2009) Joints with Inclined Screws and Steel Plates as Outer Members, In:
53 Proc. of the CIB-W18 Meeting 42, Paper No. CIB-W18/42-7-2, Dübendorf, Switzerland.
54 32
55
56
57
58
59
60

1
2
3
4
5
6
7
8
9
10
11
12
13
14
15
16
17
18
19
20
21
22
23
24
25
26
27
28
29
30
31
32
33
34
35
36
37
38
39
40
41
42
43
44
45
46
47
48
49
50
51
52
53
54
55
56
57
58
59
60

1 Matsunaga H, Miyazu Y, Soda S (2009) An universal modeling method for wooden shear/non-shear
2 walls. Journal of Structural and Construction Engineering, Transactions of AIJ : 639, 889-896
3 (in Japanese)
4 NIPPON STEEL BOLTEN CORPORATION (2019) : High Strength Hexagon Bolts – Production
5 Boucher 1. (in Japanese) http://www.bolten.co.jp/images/product/catalog/Pamphlet_1.pdf
6 (Accessed on 2019.5.01).
7 Pirnbacher G, Brandner R, Schickhofer G (2009) Base Parameters of self-tapping Screws, In: Proc.
8 of the CIB-W18 Meeting 42, Paper No. CIB-W18/42-7-1, Dübendorf, Switzerland.
9 Riberholt H (1986) Glued bolts in Glulam. Department of Structural Engineering, Technical
10 University of Denmark; Series R; Number 210
11 Ringhofer A, Brandner R, Schickhofer G (2015) Withdrawal Resistance of Self-Tapping Screws in
12 Unidirectional and Orthogonal Layered Timber Products, Materials and Structures 48: 1435–
13 1447.
14 ROTHO BLAAS SRL (2019):Wood Screw JP : (in Japanese)
15 https://issuu.com/rothoblaas/docs/2018_06_viti_giappone?e=18207635/62567172
16 (Accessed on 2019.5.01)
17 Tani S., Nomura S., Nagasawa T., Hiramatsu A (1972) Restoring Force Characteristics of
18 Reinforced Concrete Aseismic Elements (Part1) - Restoring Force Characteristics and
19 Metallization -. Transactions of Architectural Institute of Japan 202: 11-19 (in Japanese)
20 Tomasi R, Crosatti A, Piazza M (2010) Theoretical and experimental analysis of timber-to-timber
21 joints connected with inclined screws. Construction and Building Materials 24: 1560–1571.

22
23 **Appendix I**

24 **Notation**

- 25 a : Distance between the compressive axial force to the compressive resultant force (mm)
26 (Fig.9)
27 $A, B, n1$ and $n2$: Parameters governing the shape of hysteretic loop. (Equation 22)
28 B_b : Contact width of beam member (mm) (Equation 8)
29 B_s : Contact width of steel base plate (mm) (Equation 15)
30 $31.6 + 10.9 \cdot B_b$: Effective foundation depth as a function of contact width B_b (mm) (Equation (8))
31 c : Contact length (mm) (Fig.8)
32 C_r : Splitting failure constant (N/mm^{1.5}) (Equation 24)

1
2
3
4
5
6
7
8
9
10
11
12
13
14
15
16
17
18
19
20
21
22
23
24
25
26
27
28
29
30
31
32
33
34
35
36
37
38
39
40
41
42
43
44
45
46
47
48
49
50
51
52
53
54
55
56
57
58
59
60

- 1 e : Extended length of steel plate from compressive axial force (mm) (Fig.7)
- 2 E_{w0} : Modulus of elasticity of glulam parallel to the grain (N/mm²) (Equation 8)
- 3 F_s : Basic shear strength of timber (N/mm²) (Equation 23-(c))
- 4 g : Distance between tensile axial force $T P$ and compressive axial force $C P$ (mm)
- 5 (Equation 3)
- 6 h : Depth of column (mm) (Equation 23-(b))
- 7 h_e : Distance from loading side edge till far apart connector (mm) (Equation 23-(b),(c))
- 8 $T K_{ISJ45}$: Tensile rigidity of inclined screw group driven with 45 degree to the grain (kN/mm)
- 9 (Equation 5)
- 10 $T K_{SJ90}$: Tensile rigidity of screw group inserting perpendicular to the grain (kN/mm) (Equation
- 11 13)
- 12 $C K_{ISJ45}$: Compressive rigidity of inclined screw group driven with 45 degree to the grain
- 13 (kN/mm). (Equation 6)
- 14 $C K_{SJ90}$: Compressive rigidity of screw group inserting perpendicular to the grain (kN/mm)
- 15 (Equation 6)
- 16 K_{w90} : Spring constant relating to the compressive resultant force and deformation (kN/mm)
- 17 (Equation 17)
- 18 $K_{w0} = (k_{w0} \cdot B_b \cdot c)$: Spring constant (kN/mm) (Equation 9)
- 19 k_{w0} : Embedment coefficient of timber parallel to the grain (N/mm³) (Equation 7)
- 20 k_{w90} : Embedment coefficient of timber perpendicular to the grain (N/mm³). (Equation 16)
- 21 l : Width of beam (mm) (Equation 23-(b),(c))
- 22 $C P$: Compressive axial force held by inclined screw group (kN) (Equation 2)
- 23 $T P$: Tensile axial force held by inclined screw group (kN) (Equation 1)
- 24 $T P_{90}$: Tensile force received by screw group inserting perpendicular to the grain (kN)
- 25 (Equation 13)
- 26 $C P_{90}$: Compressive force received by screw group inserting perpendicular to the grain (kN)
- 27 (Equation 14)
- 28 $C_w P_{90}$: Compressive resultant force due to triangular rotational contact by steel base plate (kN)
- 29 (Equation 15)

- 1
2
3
4
5
6
7
8
9
- 10 1 ${}_c P_0$: Compressive resultant force due to “even contact” of end-grain surface of beam member
11
12 2 (kN) (Equation10)
13 3 P_{uw2} : Ultimate load carrying capacity due to shear failure (N) (Equation23-(c))
14 4 P_{uw} : Ultimate load carrying capacity due to splitting or shear failure (N) (Equation23-(a))
15 5 P_{uw1} : Ultimate load carrying capacity due to splitting failure (N) (Equation23-(b))
16 6 Q_1, Q_2 : Shear forces at both side of mechanical joint subject to tensile force P (N) (Equation
17 7 23-(c))
18 8 R_{Jb} : Rotational rigidity of the beam-side joint (kNm/rad) (Equation12)
19 9 R_{Jc} : Rotational rigidity of the column-side joint (kNm/rad) (Equation19)
20 10 R_{Jbc} : Rotational rigidity of beam-column joint (kNm/rad) (Equation21)
21 11 r_0 : Specific gravity of timber (Equation 24)
22 12 $T u_{SJ}$: Tensile deformation between steel base plate and tensile side column member (mm).
23 13 (Equation1)
24 14 ${}_c u$: Compressive deformation at the point of the resultant force (mm) (Equation7)
25 15 ${}_c u_{SJ}$: Compressive deformation of screw group in the column due to the compressive force
26 16 (mm). (Equation14)
27 17 ${}_c u_{ISJ}$: Slip deformation between steel splice plate and compressive-side beam member (mm).
28 18 (Equation4)
29 19 $T u_{ISJ}$: Slip deformation between steel splice plate and tensile-side beam member (mm).
30 20 (Equation3)
31 21 ${}_c \sigma$: Compressive stress at end-grain surface of the beam (N/mm^2) (Equation 9)
32 22 $\sigma(x)$: Compressive stress distribution assumed as triangular distribution (N/mm^2) (Equation
33 23 15)
34 24 λ_b : Distance between neutral axis $N - N'$ and the axis of compressive force ${}_c P$ in the
35 25 beam member (mm) (Equation 6)
36 26 λ_c : Distance between neutral axis $N - N'$ and the axis of compressive force ${}_c P_{90}$ in the
37 27 column member (mm) (Equation 18)
38 28 θ_b : Rotational angle defined for the beam-side joint (rad) (Fig.7)
39 29 θ_c : Rotational angle defined for the column-side joint (rad) (Fig.7)
40
41
42
43
44
45
46
47
48
49
50
51
52
53
54
55
56
57
58
59
60